Local myostatin inhibition improves skeletal muscle glucose uptake in insulin resistant high fat diet-fed mice

Article

Accepted Version

Local myostatin inhibition improves skeletal muscle glucose uptake in insulin resistant high fat diet-fed mice

Wouter Eilers[1], David Chambers[2], Mark Cleasby[3] & Keith Foster[1]

[1] School of Biological Sciences, University of Reading, United Kingdom

[2] Wolfson Centre for Age Related Diseases, King's College, University of London London, United Kingdom

[3] Royal Veterinary College, University of London, London, United Kingdom

Running head

Myostatin inhibition improves muscle glucose uptake

Author contributions

WE, MC & KF designed experiments, WE, MC & DC performed experiments, WE, MC & KF analysed data and WE wrote the paper with input from DC, MC and KF

Corresponding author:

Wouter Eilers, PhD

w.eilers@reading.ac.uk

School of Biological Sciences

Hopkins Building

Whiteknights Campus

University of Reading

Reading, RG6 6LA

United Kingdom

Abstract

Myostatin inhibition is thought to improve whole body insulin sensitivity and mitigate the development of insulin resistance in models of obesity. However, although myostatin is known to be a major regulator of skeletal muscle mass, the direct effects of myostatin inhibition in muscle on glucose uptake and the mechanisms which may underlie this are still unclear. We investigated the effect of local myostatin inhibition by adeno-associated virus-mediated overexpression of the myostatin pro-peptide on insulin-stimulated skeletal muscle glucose disposal in chow-fed or high fat diet-fed mice and evaluated the molecular pathways that might mediate this. We found that myostatin inhibition improved glucose disposal in obese high fat diet-fed mice alongside the induction of muscle hypertrophy, but did not have an impact in chow-fed mice. This improvement was not associated with greater glucose transporter or peroxisome proliferator-activated receptor gamma coactivator-1α expression or 5' AMP-activated protein kinase activation as previously suggested. Instead, transcriptomic analysis suggested that the improvement in glucose disposal was associated with significant enrichment in genes involved in fatty acid metabolism and translation of mitochondrial genes. Thus, myostatin inhibition improves muscle insulin-stimulated glucose disposal in obese high fat diet-fed mice independent of muscle hypertrophy, potentially involving previously unidentified pathways.

Keywords

Myostatin – Skeletal muscle – Glucose uptake – Insulin resistance - Diabetes

Introduction

The development of skeletal muscle insulin resistance is an important feature of type 2 diabetes because skeletal muscle is a major site of post-prandial glucose uptake. In addition, the development of insulin resistance is thought to be a feature of the loss of muscle mass during aging, known as sarcopenia. Inhibition of myostatin, a negative regulator of muscle size, has received significant attention as a potential therapeutic strategy for the improvement of both muscle strength (32) and insulin sensitivity (5), and the mitigation of the pathological features of the metabolic syndrome. Myostatin is a member of the transforming growth factor-β family of proteins that is secreted and activates Smad2/3 signalling in cells in an autocrine/paracrine fashion by binding the activin type 2A and 2B receptors (20). It is expressed predominantly in muscle and (at the mRNA level) at much lower levels in adipose tissue (1).

Knockout of the myostatin gene causes significant enlargement of skeletal muscles through both hyperplasia and hypertrophy (24), but this increase in muscle mass is not mirrored by an increase in muscle strength (2). In contrast, post-natal inhibition of myostatin causes muscle hypertrophy, but not hyperplasia, (3, 19), and results in a concomitant increase in muscle strength (12, 23). Much less is known about the effect of myostatin inhibition on muscle glucose uptake and insulin sensitivity. Myostatin gene knockout prevents fat mass gain during the lifespan of chow-fed mice (25) and most evidence indicates that the genetic loss of myostatin improves glucose tolerance and/or insulin sensitivity in mouse models of (extreme) obesity (13, 14, 40). Post-natal systemic myostatin antibody treatment increases skeletal muscle mass (4, 5, 18, 34, 39) and increases whole body insulin sensitivity in aged chow-fed mice, but not young mice being fed either regular chow or a high fat diet (5). Thus, myostatin inhibition-induced muscle hypertrophy is not always accompanied by an increase in insulin sensitivity, suggesting that hypertrophy is not sufficient and another, muscle mass-independent effect is required or that a potential threshold in the increase in muscle mass exists for an effect on insulin sensitivity to occur.

In addition, the mechanism through which myostatin acts to improve insulin sensitivity in skeletal muscle remains unclear. Systemic administration or overexpression of myostatin inhibitors affects the action of myostatin originating

from, and acting on, other tissues important for controlling whole body insulin sensitivity, such as white and brown adipose tissue (33). Thus, it remains unclear whether myostatin inhibition improves muscle insulin sensitivity in models of insulin resistance through a local effect or whether this effect is mediated by alterations in systemic factors. Myostatin inhibition has been proposed to stimulate signalling through the Akt pathway (36) and to increase 5' AMP-activated protein kinase (AMPK) activity (11, 43) in skeletal muscle. These pathways control the translocation of glucose transporters to the plasma membrane as part of insulin-dependent and insulin-independent signalling mechanisms, respectively (16, 17). In addition, we have previously shown greater expression of the GLUT1 and GLUT4 glucose transporters after local myostatin inhibition, which was associated with enhanced muscle glucose disposal in rat muscle (8). Finally, myostatin inhibition-dependent activation of an AMPK-peroxisome proliferator-activated receptor gamma coactivator (PGC)-1α pathway has been suggested to stimulate the formation of brown fat by increasing the secretion of the hormone irisin from skeletal muscle (30).

Generation of active myostatin requires cleavage and subsequent dimerization of a precursor protein. The NH_2-terminal latency-associated peptide (ProMyo) sequesters the myostatin dimer and prevents it from binding to the activin type 2A and 2B receptors (20). Here, we show that local skeletal muscle myostatin inhibition using an adeno-associated virus (AAV) expressing the ProMyo peptide increases insulin-stimulated glucose uptake in high-fat diet-fed mice, but not in chow-fed mice despite the presence of significant muscle hypertrophy. In contrast to previous work, this was not associated with increased PGC-1α or glucose transporter expression.

Methods

Preparation of adeno-associated virus

The adeno-associated virus (AAV) construct containing a modified myostatin propeptide sequence fused to a mouse immunoglobulin G2a (IgG2a) moiety under control of a CAGG promoter was as previously described (12, 41). AAV2/8 ProMyo viral particles were produced and titered by Vector Core (Nantes, France).

Animals

Male C57BL/6 mice (Harlan Laboratories) and myostatin knockout mice on a C57BL/6 background (24) were housed in animal facilities at the Royal Veterinary College or the University of Reading under a 12:12 hour day-night cycle with standard chow or a high fat diet and water available *ad libitum*. The high fat diet was obtained from Research Diets (New Brunswick, USA; #D12451), and contained 45% of calories derived from fat (lard and soy bean oil), 35% from carbohydrates and 20% from protein. All experimental procedures were carried out under a United Kingdom Home Office licence in compliance with the Animals (Scientific Procedures) Act 1986.

For intramuscular administration of AAV8 ProMyo, mice were anaesthetized with isoflurane (4% induction, 2% maintenance) and the anterior aspect of the lower limbs was shaved. AAV ProMyo ($5x10^{10}$ virus particles in 50 µl PBS-MK) was injected into the cranial compartment of the left lower leg with a 29-gauge insulin syringe, while the right leg was injected with 50 µl PBS-MK as a paired control.

Intraperitoneal insulin and glucose tolerance tests

For intraperitoneal insulin tolerance tests (IPITT), mice were fasted for 3–4 hours before administering insulin. Insulin was prepared at 100 iu/ml in normal saline and used to resuspend nitrogen-dried 2-[1,2-^{3}H(N)]-deoxy-D-glucose (0.37 MBq). Basal blood glucose was measured in tail blood with an Accu-Check Advantage meter (Roche Diagnostics, Burgess Hill, West Sussex, UK). A further 10 µl of blood was collected in microfuge tube containing 1 iu heparin in saline, mixed and placed on ice. Immediately afterwards, insulin and deoxyglucose tracer was administered intraperitoneally at a dose of 0.75 iu/kg. At 15, 30, 60 and 90 minutes after insulin

administration, blood glucose was measured as described above. After taking the final blood sample, the mice were euthanized by cervical dislocation and tibialis cranialis (TC), extensor digitorum longus, soleus muscles and epididymal fat pads were collected, weighed and frozen in liquid nitrogen-cooled isopentane. Intraperitoneal glucose tolerance test (IPGTT) was conducted and glucose clearance into TC muscle was determined as described previously (7).

In vivo study design

For the time course analysis of the effect of myostatin inhibition, 3-month-old C57BL/6 males were given an intramuscular injection of AAV ProMyo as described above, and were kept for 1, 2, 4 or 10 weeks before being subjected to an IPITT or an IPGTT, after which they were euthanized and their muscles harvested and snap-frozen (n=10 per time point).

To determine the effect of myostatin inhibition in HFD-fed mice, C57BL/6 males were switched from regular chow to high fat diet (HFD) at 8 weeks of age, while contemporaneous controls were kept on a normal chow diet. Four weeks later, mice were given intramuscular injections of AAV8 ProMyo into one TC muscle, while the contra-lateral limb was injected with saline. Mice were kept for 2 or 10 weeks post-injection, after which mice (n=10 per group) underwent an IPITT, before euthanasia and muscle collection. The remaining mice were euthanized and their muscles were harvested without undergoing an IPITT (n=8 per group).

RNA analysis

TC muscles from mice harvested without IPITT 10 weeks after AAV or saline injection were homogenized in Tri-reagent (Sigma-Aldrich) and RNA was extracted according to the manufacturer's instructions. One microgram of RNA was reverse transcribed using a qScript cDNA synthesis kit (Quanta Biosciences). Transcript levels were quantified in duplicate by real-time PCR using PerfeCta SYBR Green FastMix (Quanta Biosciences). A serial dilution of a mixture of cDNA from all samples was prepared and used to construct a standard curve for relative quantification of target transcripts, expression of which were normalized to that of

CNSK2A2, a reference gene which was defined after geNorm analysis (https://genorm.cmgg.be/). The primer sequences used are listed in Table 1.

For microarray analysis, independent pooled RNA samples were prepared by mixing 500 ng total RNA from four independent samples to create two RNA pools from both ProMyo-overexpressing and saline-injected muscle samples. Total RNA integrity for each replicate was determined using by Bioanalyzer on a RNA Pico Chip (Agilent Technologies, as per manufacturer's instructions). For microarray analysis, labelled extracts were prepared from total RNA samples using the Nugen Ovation V2 system followed by Nugen Encore Biotin Labelling Kit (Nugen Technologies Inc, as per manufacturer's instructions). Subsequently, samples were hybridized to Affymetrix Mouse 430_2 GeneChips as per manufacturer's guidelines (Nugen Technologies Inc and ThermoFisher Scientific)

Raw intensity data were processed with the RMA algorithm with quantile normalisation using the Affymetrix Expression Console software. The resulting expression data were subjected to gene set enrichment analysis (GSEA) (26, 35) using GSEA software v_3.0. Input data were the bi-weight average signal (log2). Genes without a gene symbol were excluded and data were collapsed into single gene symbols before the analysis, using the median expression value for each gene symbol (20630 genes remained). All genes were ranked on the basis of differential expression between ProMyo and saline-injected muscles, defined as the real values of Diff_of_Classes. Three separate GSEA runs were performed; one with the gene sets KEGG_FATTY_ACID_METABOLISM, KEGG_OXIDATIVE_PHOSPHORYLATION and KEGG_INSULIN_SIGNALING_PATHWAY, one with ten gene sets related to inflammation (see table 2) and one with collection c5.all.v6.1, a collection of 5,917 gene sets based on gene ontologies. All gene sets were obtained from Molecular Signature Database v6.1. GSEAs were run with permutation of gene sets (n=1,000), using the weighted enrichment statistic, and default parameters for gene set size (minimum size 15, maximum size 500). A false discovery rate of <0.05 was accepted as being significant. Subsequent Leading Edge Analysis was performed to determine overlap between significantly enriched gene sets in genes mostly responsible for the enrichment score.

The microarray data have been uploaded to Gene Expression Omnibus (accession GSE130622). Output enrichment plots for gene sets listed in table 2 are available upon request.

Western blotting

Liquid nitrogen-powdered muscle was lysed in cold RIPA buffer (50 mM TRIS-HCl (pH 7.5), 150 mM NaCl, 1 mM EDTA, 1% v/v Nonidet P40 substitute, 0.25% sodium deoxycholate, plus freshly added protease inhibitor cocktail (Sigma), phosphatase inhibitor cocktail (Sigma) and 20 mM beta-glycerophosphate). Protein concentration was determined using the Bio-rad DC protein assay. Samples were adjusted to the same concentration with RIPA buffer and SDS-PAGE loading buffer containing beta-mercaptoethanol (2% final concentration) was added. Samples containing 40 µg protein were separated on pre-cast 4–12% Bis-Tris gels (Life Technologies) and blotted onto PVDF membranes. Membranes were blocked in 5% non-fat dried milk in Tris-buffered saline with 0.5% tween-20 (TBS-T) and incubated overnight at 4°C with primary antibody diluted in TBS-T, 5% BSA. Membranes were subsequently incubated with horseradish-conjugated species-specific secondary antibodies (Millipore) in TBS-T containing 5% non-fat milk powder. Membranes were washed 3 × 5 min in TBS-T after each step. Antibodies were then detected with ECL Plus (Bio-rad) and an ImageQuant LAS4000 mini (GE Healthcare). The following primary antibodies were used: anti-Akt #9272, anti-pSer473-Akt #9271, anti-AMPKα #2532, anti-pThr172-AMPKα, anti-ACC #3662, anti-pSer79-ACC #3661, anti-α-actinin #6487, anti-GAPDH #5174 and anti-Cblb #9498 from Cell Signaling Technology; anti-PGC-1α #54481 and OXPHOS antibody cocktail #110413 from Abcam; and anti-GLUT4 #sc-53566 from Santa Cruz Biotechnology.

Statistical analysis

Statistical analyses were carried out using SigmaPlot v12.3 or GraphPad Prism v6. Data from time course experiments, and experiments involving different diets and myostatin inhibition were analysed with Two-Way Repeated Measures ANOVA, with time or myostatin inhibition as the paired factor. The Sidak-Holm method was used for *post-hoc* testing. Two-group comparisons were performed using *t*-tests, after verifying equality of variance and normality. The threshold for statistical significance

244 was set at $p<0.05$. Data are displayed as mean ± standard error of the mean
245 (S.E.M), or as mean plus individual data points.
246

Results

Myostatin inhibition increases muscle size, but not insulin-stimulated glucose disposal in chow-fed mice

Overexpression of ProMyo in TC muscles of chow-fed mice for 1, 2, 4 or 10 weeks resulted in significant muscle hypertrophy in wild-type mice (Figure 1A) but not in myostatin knockout mice (Figure 1B). As expected, muscle mass was substantially higher in the myostatin knockout mice compared to the wild type mice (Figure 1A &1B). However, inhibition of the activin type 2B receptor has been shown to lead to additional hypertrophy in myostatin knockout mice (21) and the absence of such an effect of AAV ProMyo on muscle mass in the knockout mice implies that the construct is myostatin-specific. Insulin-stimulated glucose disposal, as measured by IPITT, was not different between saline- and AAV ProMyo-injected muscles at any of the time points (Figure 1C). Total glucose uptake into muscle was higher after 4 and 10 weeks ProMyo overexpression by virtue of the significant increases in muscle mass (Figure 1D). As we have previously demonstrated higher muscle glucose uptake per unit muscle mass in ProMyo overexpressing rat muscle during a glucose tolerance test (IPGTT) (8), we measured glucose uptake during an IPGTT in mice after two weeks of ProMyo overexpression. However, we found no difference in glucose uptake between saline and AAV-ProMyo-injected muscles (Figure 1E). These data suggest that although myostatin inhibition-induced muscle hypertrophy increases total glucose disposal into muscle under conditions of hyperinsulinaemia, muscle glucose uptake per unit muscle mass is not increased by myostatin inhibition in chow-fed mice.

Myostatin inhibition increases insulin-stimulated glucose disposal in muscle of HFD-fed mice

We next investigated whether local myostatin inhibition would improve muscle glucose uptake in HFD-fed mice. Mice were given an intramuscular injection of AAV8 ProMyo or saline after 4 weeks of HFD-feeding. One group of mice was analysed after 2 weeks of myostatin inhibition (6-week total duration of HFD). At this time point, total body mass was not significantly greater in the HFD-fed mice (Figure 2A), but epididymal fat pad mass was significantly increased (Figure 2B), indicating visceral fat accumulation. We did not detect a significant difference in fasting or

IPITT blood glucose levels between diet groups (Figure 2C), but HFD-fed mice displayed a delayed reduction in blood glucose levels in response to insulin (Figure 2D), which is indicative of whole body insulin resistance. AAV8 ProMyo-injected TC muscles from both chow- and HFD-fed mice showed significant hypertrophy (+9.7% and +8.8% *vs*. saline, respectively; Figure 2E). However, neither chow-fed nor HFD-fed mice showed an increase in glucose uptake into ProMyo-overexpressing TC muscles (Figure 2F). These data suggest that 2 weeks of myostatin inhibition in muscle is not sufficient to significantly increase insulin-stimulated glucose disposal in muscles of HFD-fed mice.

After 10 weeks of myostatin inhibition (14 weeks of HFD-feeding), we observed a more severe metabolic phenotype. A significant increase in total body mass was detected (Figure 3A) and fat pad mass had increased to a greater extent in HFD-fed mice (Figure 3B). In addition, HFD-fed mice showed significantly higher fasting glucose levels than chow-fed controls and had a clearly delayed response to insulin during the IPITT (Figure 3C and 3D). Muscle mass was substantially greater in ProMyo overexpressing muscles than in saline-treated controls in both chow (+22.8%) and HFD (+23.2%) groups (Figure 3E). At this time point the ProMyo overexpressing muscles of the insulin-resistant HFD-fed mice showed significantly higher glucose uptake per unit mass during the IPITT than saline-injected controls (by ~78%) (Figure 3F). On this basis, total muscle glucose disposal can be estimated to be increased by 115–121% of that of control muscles. Taken together, these data suggest that 10 weeks of myostatin inhibition in mouse muscle specifically increases insulin-stimulated muscle glucose disposal in HFD-fed, but not chow-fed mice, despite the presence of significant muscle hypertrophy in both groups of mice.

Effect of myostatin inhibition on potential regulators of insulin sensitivity

We next determined whether myostatin inhibition selectively induced changes in pathways controlling GLUT translocation and/or expression in HFD-fed mice. Muscles from mice not subjected to IPITT were used for the analysis. Measurement of pro-myostatin mRNA, which includes the sequence for the inhibitory ProMyo peptide, showed robust overexpression of the ProMyo construct in muscles of chow- and HFD-fed mice after 10 weeks of myostatin inhibition (87±16-fold & 57±9-fold, respectively, Figure 4A). Slc2a1/GLUT1 mRNA levels were lower in ProMyo-

overexpressing muscles (Figure 4B). Slc2a4/GLUT4 mRNA levels were significantly lower in ProMyo-overexpressing muscles of HFD-fed mice compared to ProMyo-overexpressing muscles of chow-fed mice (Figure 4C). GLUT1 and GLUT4 protein levels did not differ among any of the groups (Figure 4D-4F). These data suggest that, unexpectedly, GLUT expression was unaltered or reduced at the transcript level by myostatin inhibition. Basal Ser473 phosphorylation of Akt and Thr172 phosphorylation of AMPKα were similar between diet groups or in ProMyo-overexpressing muscles (Figure 5A & 5C). However, Akt protein levels were increased in ProMyo-overexpressing muscles of chow-fed mice, but not of HFD-fed mice (Figure 5B). AMPKα protein levels did not differ among the groups (Figure 5D). Likewise, basal Ser79 phosphorylation of acetyl-CoA carboxylase (ACC), which is indicative of AMPK activity, was similar among the groups (Figure 5E). ACC expression was increased in ProMyo-overexpressing muscles, although there was no significant difference within individual diet groups (Figure 5F). PGC-1α protein levels were significantly higher in HFD-fed mice but there was no effect of ProMyo overexpression (Figure 5G). These data suggest that the basal activities of pathways controlling GLUT expression and translocation were not specifically upregulated in HFD-fed mice by ProMyo overexpression.

We explored the possibility that myostatin inhibition affects the expression of two more recently identified regulators of both myogenesis and muscle insulin sensitivity. Mitsugumin 53 (MG53) and Casitas B-cell lymphoma-b (Cbl-b) are E3 ligases that target the insulin receptor substrate 1 (IRS-1) for proteasomal degradation and their expression is thought to inhibit myoblast differentiation (42) and induce muscle atrophy during muscle unloading (29). Furthermore, MG53 is thought to induce muscle insulin resistance in response to high fat diet-feeding (31). Unexpectedly, transcript levels of MG53 were unaffected by HFD-feeding and were higher in ProMyo overexpressing muscles (Figure 6A). Cbl-b mRNA expression was not affected by ProMyo overexpression (Figure 6B), but its protein level was lower in HFD-fed mice (Figure 6C & 6D). Together, these data suggest unexpected changes in the expression of MG53 and Cbl-b in response to both high fat-diet feeding and myostatin inhibition that are unlikely to explain the observed effects on insulin-stimulated muscle glucose disposal.

Mitochondrial ribosomal protein transcripts are enriched after myostatin inhibition

To obtain insight into possible alternative mechanisms for the effect of myostatin inhibition on skeletal muscle glucose uptake, we performed GSEA on transcriptomic data obtained from muscles from HFD-fed mice subjected to 10 weeks of myostatin inhibition and their paired saline-injected controls. We detected a 600-fold increase in IgG2A expression, which was due to the presence of IgG2A sequence in the AAV ProMyo-Fc construct. Therefore, this transcript was removed from the GSEA. To explain the observed increase in glucose uptake, we hypothesized that genes related to insulin signaling, fatty acid metabolism and oxidative phosphorylation may be enriched in the ProMyo overexpressing muscles. We detected significant enrichment of the KEGG_FATTY_ACID_METABOLISM gene set, but not of the KEGG_INSULIN_SIGNALING_PATHWAY or KEGG_OXIDATIVE_PHOSPHORYLATION gene sets (Table 2 & Table 3). It has been suggested that the effect of myostatin inhibition on glucose uptake in HFD-fed mice can be explained by reduced muscle inflammation (11). Therefore, we determined the enrichment of gene sets related to inflammation in our muscle samples. However, none of these gene sets showed significant enrichment in either saline-treated or ProMyo-overexpressing muscles (Table 2).

To explore possible novel pathways involved in mediating the effect of myostatin inhibition on muscle glucose uptake, we repeated the GSEA with a large collection of gene sets based on gene ontologies. We found four gene sets that were enriched in ProMyo overexpressing muscles at a FDR of <5% (Table 2). These gene sets show a significant amount of overlap in that all contain mitochondrial ribosomal proteins. Subsequent analysis of the overlap in the genes responsible for the significant enrichment scores indeed mostly identified genes encoding mitochondrial ribosomal proteins and other genes involved in mitochondrial translation (Table 4), suggesting that myostatin inhibition increases the expression of these genes in the muscle of HFD-fed mice. Because the transcriptomic data suggest that the translation of mitochondrial DNA-encoded genes might be specifically enhanced, we analysed the protein levels of the nuclear DNA-encoded ubiquinol-cytochrome c reductase core protein 2 (UQCRC2) and succinate dehydrogenase complex iron sulfur subunit B (SDHB), and the mitochondrial DNA-encoded cytochrome c oxidase I (MTCO1). However, we found no differences in either the nuclear or mitochondrially encoded oxidative phosphorylation complex subunits among the groups (Figure 7).

Discussion

Myostatin inhibition is thought to improve muscle glucose disposal but the mechanisms whereby this is achieved and their quantitative importance are unclear. We show here that myostatin inhibition increases insulin-stimulated glucose disposal in skeletal muscle of HFD-fed mice, but not chow-fed mice, at a time point at which substantial muscle hypertrophy had occurred. Unexpectedly, this was not associated with higher expression of GLUT1/GLUT4 or PGC-1α, or basal phosphorylation of Akt or AMPK, which have been proposed to be regulators of the positive effects of myostatin inhibition on insulin sensitivity. However, we observed significant enrichment of genes involved in fatty acid metabolism and mitochondrial translation following myostatin inhibition.

The lack of an effect of local myostatin inhibition on muscle insulin-stimulated glucose disposal in chow-fed mice was unexpected. Beneficial effects on glucose uptake and insulin sensitivity have been observed in multiple models of genetically induced muscle hypertrophy (6, 9, 10), implying the possibility of a common mechanism that leads to greater muscle glucose uptake. Furthermore, our previous experiments in rats demonstrated greater glucose disposal during an IPGTT after 17 days of overexpression of the same ProMyo-Fc construct, which was associated with increased expression of GLUT1 and GLUT4 (8). However, muscle glucose uptake per unit muscle mass during an IPITT was unchanged throughout the full time course of the development of muscle hypertrophy (Figure 1C). This demonstrates that increases in muscle glucose disposal rate are not the inevitable result of myostatin inhibition-induced muscle hypertrophy.

We observed significantly higher insulin-stimulated glucose disposal in ProMyo overexpressing muscles after 10 weeks, but not 2 weeks, of local myostatin inhibition in mice on an HFD (Figure 2F & 3F). The mice from the 10 week time point showed a more severe metabolic phenotype as a result of a longer duration of HFD feeding, with further increases in visceral fat accumulation, high fasting blood glucose and clear insulin resistance compared to the chow-fed mice and the two week time point (Figure 2 & 3). Despite this, glucose uptake was not lower in the muscles of the HFD-fed mice compared to those of the chow-fed mice (Figure 2F & 3F). Other

groups have shown that feeding C57Bl/6 mice a similar HFD (i.e. 45% of calories from fat) for a similar or shorter amount of time leads to insulin resistance in TC muscle (37). The IPITT method we used to measure muscle glucose uptake involves a significant amount of variation between animals which can make it difficult to detect between-animal effects such as those of the diet.

Nevertheless, our data suggest that the beneficial effect of myostatin inhibition on muscle glucose disposal requires a muscle hypertrophy-independent factor, which may be associated with the development of a severe metabolic phenotype. We have previously shown that local myostatin inhibition increases muscle glucose disposal to a much greater extent than muscle size in chow-fed rats (8), suggesting this factor may not be exclusively related to metabolic disease. Myostatin antibody treatment resulted in muscle hypertrophy in chow- and HFD-fed young mice and chow-fed old mice, but only increased whole body insulin sensitivity in the old mice (5). The absence of improvements in insulin sensitivity in young mice in the experiments by Camporez *et al.* might be explained by a requirement for a minimum level of hypertrophy in combination with the presence of a significant metabolic phenotype, as the mice from the 2 week myostatin inhibition time point in our study displayed a similar degree of hypertrophy, had been fed a HFD for a similar duration, and displayed no increase in glucose disposal with myostatin inhibition (Figure 2). However, it is unclear why an improvement was observed in old mice despite the presence of a similar degree of muscle hypertrophy in young mice.

Together these data suggest that an increase in insulin-stimulated glucose disposal into muscle by postnatal myostatin inhibition in young mice requires a significant metabolic phenotype combined with a long duration of inhibition, although rats appear to be more sensitive to the effects of myostatin inhibition (8). The reason for the difference in the effect of ProMyo overexpression in chow-fed mice and rats is unclear. Our chow-fed mouse data set (Figure 1) includes a time point that is similar to the time point used in our previous rat study, at which the degree of hypertrophy was similar and at which we assessed glucose uptake during both an IPITT and an IPGTT, which was the test performed in the rats. It is possible that the larger content of the more insulin-sensitive type 1/2A muscle fibres in the rat TC muscle compared to that of the mouse TC muscle (~5/25% vs ~0/5%, respectively) played a role in the different response to myostatin inhibition, and that local myostatin inhibition in a

mouse muscle with a fibre type composition more similar to that of the rat TC would have shown a similar increase in glucose uptake.

The data have potential implications for the clinical translation of myostatin inhibition for the treatment of insulin resistance, as it may be that more obese individuals are more likely to benefit from myostatin inhibitors. Obesity does not appear to affect the degree of muscle hypertrophy resulting from myostatin inhibition (Figure 3E), and indeed the magnitude of the increase in insulin-stimulated glucose disposal exceeds that of the increase in muscle mass (Figure 3F). Thus, myostatin inhibition leads to substantial improvements in total insulin-stimulated muscle glucose disposal, which implies a treatment strategy utilising this approach would have positive effects in obese insulin resistant patients.

Among the potential mechanisms which have been suggested to explain the positive effects of myostatin inhibition on muscle or whole body glucose uptake are higher expression of glucose transporters GLUT1 and GLUT4 (8), activation of Akt (27, 36), and stimulation of brown fat formation by increasing the secretion of the hormone irisin from skeletal muscle through an AMPK-PGC-1α-dependent mechanism (30). We did not demonstrate higher expression of any of these molecules in the ProMyo-overexpressing TC muscles from HFD-fed mice (Figure 4 & 5), and we found no evidence of increased basal AMPK activity (Figure 5). However, we cannot exclude the possibility that GLUT translocation from the cytosol to the plasma membrane was increased separately of any effect on GLUT expression. There was an increase in PGC-1α protein levels in HFD mice, which is consistent with the existing literature (15), but there was no effect of ProMyo overexpression (Figure 5G). This brings into question whether myostatin inhibition in muscle is sufficient to increase PGC-1α expression. In support of this, lower PGC-1α protein levels have been detected in myostatin knockout mice (22) and lower PGC-1α transcript levels were found in mice treated with AAV ProMyo (28). In addition, we detected no increase in expression of the insulin receptor-targeting E3 ligases MG53 and Cbl-b in HFD-fed mice, while myostatin inhibition unexpectedly increased the expression of MG53, which has previously been suggested to be responsible for muscle insulin resistance in response to HFD feeding (31) (Figure 6). Together, these data suggest that whole body insulin resistance was not associated with higher expression of these IRS-1-

485 targeting E3 ligases in muscle and that the improvement of muscle glucose disposal
486 resulting from myostatin inhibition was not associated with a decrease in their
487 expression.
488
489 The results of our experiments are contrasting with existing hypotheses regarding
490 the mechanism through which myostatin might increase skeletal muscle glucose
491 disposal, and therefore suggest that other mechanisms exist. In accordance with
492 previous observations (11) we found enrichment of gene sets associated with fatty
493 acid (FA) oxidation including acyl-CoA synthases and acyl-CoA dehydrogenases
494 (Table 2 & 3), which catalyse the initial steps in the beta-oxidation of FAs. We
495 speculate that higher expression of these sets of genes could lead to improved
496 metabolism of fatty acids, and thus greater insulin sensitivity. For example, an
497 increase in carnitine palmitoyl transferase 1 (CPT1) activity (one of the genes which
498 showed increased expression in ProMyo-overexpressing muscles) in skeletal muscle
499 improves insulin sensitivity in HFD-fed mice (38). In addition, we observed
500 enrichment of genes involved in mitochondrial translation, including those expressing
501 mitochondrial ribosomal proteins, following myostatin inhibition in muscles of HFD-
502 fed mice (Table 2 & 4). Reductions in OXPHOS gene expression in human muscle
503 have been associated with type 2 diabetes (26), but we found no significant
504 enrichment of a gene set related to oxidative phosphorylation with myostatin
505 inhibition (Table 2). In accordance with this, we found no difference in the protein
506 levels of two nuclear-encoded subunits of oxidative phosphorylation complexes
507 (Figure 7A & 7B). The protein levels of a mitochondrially encoded protein also did
508 not differ between saline-treated and ProMyo-overexpressing muscles (Figure 7C),
509 which argues against a general increase in translation of mitochondrial proteins.
510 Although any causal relationship between myostatin inhibition, changes in
511 mitochondrial gene expression and improvements in muscle glucose uptake requires
512 further investigation, it is possible that an enhancement in mitochondrial translation
513 could explain why myostatin inhibition potentiates the effects of exercise on whole-
514 body insulin sensitivity and running distance in aged mice (18).
515
516 We conclude that local post-natal myostatin inhibition improves insulin-stimulated
517 muscle glucose disposal in obese HFD-fed mice. This is not secondary to muscle
518 hypertrophy and is not observed in young insulin-sensitive mice. This effect does not

appear to rely on the upregulation of glucose transporter and PGC-1α expression but was associated with expression changes in previously unidentified pathways related to mitochondrial function. These findings point towards further areas for future investigations into the mechanism of the effects of myostatin inhibition, and suggest that therapeutic myostatin inhibition may be effective in improving muscle glucose uptake primarily in obese insulin-resistant individuals.

Acknowledgments

We thank Dr Ketan Patel (University of Reading, United Kingdom) for supplying the myostatin knockout mice.

Grants

This work was funded by a Diabetes UK Alec and Beryl Warren Award (BDA 13/0004683) to KF and MC.

Disclosures

The authors have no conflict of interest to declare.

References

1. **Allen DL, Cleary AS, Speaker KJ, Lindsay SF, Uyenishi J, Reed JM, Madden MC, and Mehan RS**. Myostatin, Activin Receptor IIb, and Follistatin-Like-3 Gene Expression is Altered in Adipose Tissue and Skeletal Muscle of Obese Mice. *Am J Physiol Endocrinol Metab* 2008.
2. **Amthor H, Macharia R, Navarrete R, Schuelke M, Brown SC, Otto A, Voit T, Muntoni F, Vrbova G, Partridge T, Zammit P, Bunger L, and Patel K**. Lack of myostatin results in excessive muscle growth but impaired force generation. *Proc Natl Acad Sci U S A* 104: 1835-1840, 2007.
3. **Amthor H, Otto A, Vulin A, Rochat A, Dumonceaux J, Garcia L, Mouisel E, Hourde C, Macharia R, Friedrichs M, Relaix F, Zammit PS, Matsakas A, Patel K, and Partridge T**. Muscle hypertrophy driven by myostatin blockade does not require stem/precursor-cell activity. *Proc Natl Acad Sci U S A* 106: 7479-7484, 2009.
4. **Bernardo BL, Wachtmann TS, Cosgrove PG, Kuhn M, Opsahl AC, Judkins KM, Freeman TB, Hadcock JR, and LeBrasseur NK**. Postnatal PPARdelta activation and myostatin inhibition exert distinct yet complimentary effects on the metabolic profile of obese insulin-resistant mice. *PLoS ONE* 5: e11307, 2010.
5. **Camporez JP, Petersen MC, Abudukadier A, Moreira GV, Jurczak MJ, Friedman G, Haqq CM, Petersen KF, and Shulman GI**. Anti-myostatin antibody increases muscle mass and strength and improves insulin sensitivity in old mice. *Proc Natl Acad Sci U S A* 113: 2212-2217, 2016.
6. **Christoffolete MA, Silva WJ, Ramos GV, Bento MR, Costa MO, Ribeiro MO, Okamoto MM, Lohmann TH, Machado UF, Musaro A, and Moriscot AS**. Muscle IGF-1-induced skeletal muscle hypertrophy evokes higher insulin sensitivity and carbohydrate use as preferential energy substrate. *BioMed research international* 2015: 282984, 2015.
7. **Cleasby ME, Davey JR, Reinten TA, Graham MW, James DE, Kraegen EW, and Cooney GJ**. Acute bidirectional manipulation of muscle glucose uptake by in vivo electrotransfer of constructs targeting glucose transporter genes. *Diabetes* 54: 2702-2711, 2005.
8. **Cleasby ME, Jarmin S, Eilers W, Elashry M, Andersen DK, Dickson G, and Foster K**. Local overexpression of the myostatin propeptide increases glucose transporter expression and enhances skeletal muscle glucose disposal. *Am J Physiol Endocrinol Metab* 306: E814-823, 2014.
9. **Cleasby ME, Reinten TA, Cooney GJ, James DE, and Kraegen EW**. Functional studies of Akt isoform specificity in skeletal muscle in vivo; maintained insulin sensitivity despite reduced insulin receptor substrate-1 expression. *Mol Endocrinol* 21: 215-228, 2007.
10. **Diaz M, Martel N, Fitzsimmons RL, Eriksson NA, Cowin GJ, Thomas GP, Cao KA, Muscat GE, and Leong GM**. Ski overexpression in skeletal muscle modulates genetic programs that control susceptibility to diet-induced obesity and insulin signaling. *Obesity (Silver Spring, Md)* 20: 2157-2167, 2012.
11. **Dong J, Dong Y, Dong Y, Chen F, Mitch WE, and Zhang L**. Inhibition of myostatin in mice improves insulin sensitivity via irisin-mediated cross talk between muscle and adipose tissues. *International journal of obesity (2005)* 40: 434-442, 2016.

12. **Foster K, Graham IR, Otto A, Foster H, Trollet C, Yaworsky PJ, Walsh FS, Bickham D, Curtin NA, Kawar SL, Patel K, and Dickson G**. Adeno-associated virus-8-mediated intravenous transfer of myostatin propeptide leads to systemic functional improvements of slow but not fast muscle. *Rejuvenation Res* 12: 85-94, 2009.
13. **Guo T, Jou W, Chanturiya T, Portas J, Gavrilova O, and McPherron AC**. Myostatin inhibition in muscle, but not adipose tissue, decreases fat mass and improves insulin sensitivity. *PLoS ONE* 4: e4937, 2009.
14. **Hamrick MW, Pennington C, Webb CN, and Isales CM**. Resistance to body fat gain in 'double-muscled' mice fed a high-fat diet. *International journal of obesity (2005)* 30: 868-870, 2006.
15. **Hancock CR, Han DH, Chen M, Terada S, Yasuda T, Wright DC, and Holloszy JO**. High-fat diets cause insulin resistance despite an increase in muscle mitochondria. *Proc Natl Acad Sci U S A* 105: 7815-7820, 2008.
16. **Klip A, Sun Y, Chiu TT, and Foley KP**. Signal transduction meets vesicle traffic: the software and hardware of GLUT4 translocation. *Am J Physiol Cell Physiol* 306: C879-886, 2014.
17. **Kurth-Kraczek EJ, Hirshman MF, Goodyear LJ, and Winder WW**. 5' AMP-activated protein kinase activation causes GLUT4 translocation in skeletal muscle. *Diabetes* 48: 1667-1671, 1999.
18. **LeBrasseur NK, Schelhorn TM, Bernardo BL, Cosgrove PG, Loria PM, and Brown TA**. Myostatin inhibition enhances the effects of exercise on performance and metabolic outcomes in aged mice. *The journals of gerontology Series A, Biological sciences and medical sciences* 64: 940-948, 2009.
19. **Lee SJ, Huynh TV, Lee YS, Sebald SM, Wilcox-Adelman SA, Iwamori N, Lepper C, Matzuk MM, and Fan CM**. Role of satellite cells versus myofibers in muscle hypertrophy induced by inhibition of the myostatin/activin signaling pathway. *Proc Natl Acad Sci U S A* 109: E2353-2360, 2012.
20. **Lee SJ, and McPherron AC**. Regulation of myostatin activity and muscle growth. *Proc Natl Acad Sci U S A* 98: 9306-9311., 2001.
21. **Lee SJ, Reed LA, Davies MV, Girgenrath S, Goad ME, Tomkinson KN, Wright JF, Barker C, Ehrmantraut G, Holmstrom J, Trowell B, Gertz B, Jiang MS, Sebald SM, Matzuk M, Li E, Liang LF, Quattlebaum E, Stotish RL, and Wolfman NM**. Regulation of muscle growth by multiple ligands signaling through activin type II receptors. *Proc Natl Acad Sci U S A* 102: 18117-18122, 2005.
22. **Lipina C, Kendall H, McPherron AC, Taylor PM, and Hundal HS**. Mechanisms involved in the enhancement of mammalian target of rapamycin signalling and hypertrophy in skeletal muscle of myostatin-deficient mice. *FEBS Lett* 584: 2403-2408, 2010.
23. **Matsakas A, Foster K, Otto A, Macharia R, Elashry MI, Feist S, Graham I, Foster H, Yaworsky P, Walsh F, Dickson G, and Patel K**. Molecular, cellular and physiological investigation of myostatin propeptide-mediated muscle growth in adult mice. *Neuromuscul Disord* 19: 489-499, 2009.
24. **McPherron AC, Lawler AM, and Lee SJ**. Regulation of skeletal muscle mass in mice by a new TGF-beta superfamily member. *Nature* 387: 83-90., 1997.
25. **McPherron AC, and Lee SJ**. Suppression of body fat accumulation in myostatin-deficient mice. *J Clin Invest* 109: 595-601, 2002.
26. **Mootha VK, Lindgren CM, Eriksson KF, Subramanian A, Sihag S, Lehar J, Puigserver P, Carlsson E, Ridderstrale M, Laurila E, Houstis N, Daly MJ, Patterson N, Mesirov JP, Golub TR, Tamayo P, Spiegelman B, Lander ES,**

Hirschhorn JN, Altshuler D, and Groop LC. PGC-1alpha-responsive genes involved in oxidative phosphorylation are coordinately downregulated in human diabetes. *Nat Genet* 34: 267-273, 2003.
27. **Morissette MR, Cook SA, Buranasombati C, Rosenberg MA, and Rosenzweig A**. Myostatin inhibits IGF-I-induced myotube hypertrophy through Akt. *Am J Physiol Cell Physiol* 297: C1124-1132, 2009.
28. **Mouisel E, Relizani K, Mille-Hamard L, Denis R, Hourde C, Agbulut O, Patel K, Arandel L, Morales-Gonzalez S, Vignaud A, Garcia L, Ferry A, Luquet S, Billat V, Ventura-Clapier R, Schuelke M, and Amthor H**. Myostatin is a key mediator between energy metabolism and endurance capacity of skeletal muscle. *Am J Physiol Regul Integr Comp Physiol* 307: R444-454, 2014.
29. **Nakao R, Hirasaka K, Goto J, Ishidoh K, Yamada C, Ohno A, Okumura Y, Nonaka I, Yasutomo K, Baldwin KM, Kominami E, Higashibata A, Nagano K, Tanaka K, Yasui N, Mills EM, Takeda S, and Nikawa T**. Ubiquitin ligase Cbl-b is a negative regulator for insulin-like growth factor 1 signaling during muscle atrophy caused by unloading. *Molecular and cellular biology* 29: 4798-4811, 2009.
30. **Shan T, Liang X, Bi P, and Kuang S**. Myostatin knockout drives browning of white adipose tissue through activating the AMPK-PGC1alpha-Fndc5 pathway in muscle. *FASEB J* 27: 1981-1989, 2013.
31. **Song R, Peng W, Zhang Y, Lv F, Wu HK, Guo J, Cao Y, Pi Y, Zhang X, Jin L, Zhang M, Jiang P, Liu F, Meng S, Zhang X, Jiang P, Cao CM, and Xiao RP**. Central role of E3 ubiquitin ligase MG53 in insulin resistance and metabolic disorders. *Nature* 494: 375-379, 2013.
32. **St Andre M, Johnson M, Bansal PN, Wellen J, Robertson A, Opsahl A, Burch PM, Bialek P, Morris C, and Owens J**. A mouse anti-myostatin antibody increases muscle mass and improves muscle strength and contractility in the mdx mouse model of Duchenne muscular dystrophy and its humanized equivalent, domagrozumab (PF-06252616), increases muscle volume in cynomolgus monkeys. *Skelet Muscle* 7: 25, 2017.
33. **Steculorum SM, Ruud J, Karakasilioti I, Backes H, Engstrom Ruud L, Timper K, Hess ME, Tsaousidou E, Mauer J, Vogt MC, Paeger L, Bremser S, Klein AC, Morgan DA, Frommolt P, Brinkkotter PT, Hammerschmidt P, Benzing T, Rahmouni K, Wunderlich FT, Kloppenburg P, and Bruning JC**. AgRP Neurons Control Systemic Insulin Sensitivity via Myostatin Expression in Brown Adipose Tissue. *Cell* 165: 125-138, 2016.
34. **Stolz LE, Li D, Qadri A, Jalenak M, Klaman LD, and Tobin JF**. Administration of myostatin does not alter fat mass in adult mice. *Diabetes, obesity & metabolism* 10: 135-142, 2008.
35. **Subramanian A, Tamayo P, Mootha VK, Mukherjee S, Ebert BL, Gillette MA, Paulovich A, Pomeroy SL, Golub TR, Lander ES, and Mesirov JP**. Gene set enrichment analysis: a knowledge-based approach for interpreting genome-wide expression profiles. *Proc Natl Acad Sci U S A* 102: 15545-15550, 2005.
36. **Trendelenburg AU, Meyer A, Rohner D, Boyle J, Hatakeyama S, and Glass DJ**. Myostatin reduces Akt/TORC1/p70S6K signaling, inhibiting myoblast differentiation and myotube size. *Am J Physiol Cell Physiol* 296: C1258-1270, 2009.
37. **Turner N, Kowalski GM, Leslie SJ, Risis S, Yang C, Lee-Young RS, Babb JR, Meikle PJ, Lancaster GI, Henstridge DC, White PJ, Kraegen EW, Marette A, Cooney GJ, Febbraio MA, and Bruce CR**. Distinct patterns of tissue-specific lipid accumulation during the induction of insulin resistance in mice by high-fat feeding. *Diabetologia* 56: 1638-1648, 2013.

38. **Vavrova E, Lenoir V, Alves-Guerra MC, Denis RG, Castel J, Esnous C, Dyck JR, Luquet S, Metzger D, Bouillaud F, and Prip-Buus C**. Muscle expression of a malonyl-CoA-insensitive carnitine palmitoyltransferase-1 protects mice against high-fat/high-sucrose diet-induced insulin resistance. *Am J Physiol Endocrinol Metab* 311: E649-660, 2016.
39. **Whittemore LA, Song K, Li X, Aghajanian J, Davies M, Girgenrath S, Hill JJ, Jalenak M, Kelley P, Knight A, Maylor R, O'Hara D, Pearson A, Quazi A, Ryerson S, Tan XY, Tomkinson KN, Veldman GM, Widom A, Wright JF, Wudyka S, Zhao L, and Wolfman NM**. Inhibition of myostatin in adult mice increases skeletal muscle mass and strength. *Biochem Biophys Res Commun* 300: 965-971, 2003.
40. **Wilkes JJ, Lloyd DJ, and Gekakis N**. A loss of function mutation in myostatin reduces TNF{alpha} production and protectsliver against obesity induced insulin resistance. *Diabetes* 2009.
41. **Wolfman NM, McPherron AC, Pappano WN, Davies MV, Song K, Tomkinson KN, Wright JF, Zhao L, Sebald SM, Greenspan DS, and Lee SJ**. Activation of latent myostatin by the BMP-1/tolloid family of metalloproteinases. *Proc Natl Acad Sci U S A* 100: 15842-15846, 2003.
42. **Yi JS, Park JS, Ham YM, Nguyen N, Lee NR, Hong J, Kim BW, Lee H, Lee CS, Jeong BC, Song HK, Cho H, Kim YK, Lee JS, Park KS, Shin H, Choi I, Lee SH, Park WJ, Park SY, Choi CS, Lin P, Karunasiri M, Tan T, Duann P, Zhu H, Ma J, and Ko YG**. MG53-induced IRS-1 ubiquitination negatively regulates skeletal myogenesis and insulin signalling. *Nat Commun* 4: 2354, 2013.
43. **Zhang C, McFarlane C, Lokireddy S, Bonala S, Ge X, Masuda S, Gluckman PD, Sharma M, and Kambadur R**. Myostatin-deficient mice exhibit reduced insulin resistance through activating the AMP-activated protein kinase signalling pathway. *Diabetologia* 54: 1491-1501, 2011.

Figure 1: AAV8 ProMyo increases muscle mass but not insulin-stimulated glucose disposal in chow-fed mice

A: Mass of saline- or AAV8 ProMyo-injected tibialis cranialis (TC) muscle at 1, 2, 4 & 10 weeks post-injection (n=10 per group). B: TC muscle masses of 2-month-old myostatin null mice 4 weeks after a single intramuscular injection of AAV8 ProMyo (n=3 per group). C: Glucose uptake per unit muscle mass during an intraperitoneal (i/p) insulin tolerance test (IPITT) at the indicated times after saline or AAV8 ProMyo injection. D: Total muscle glucose uptake at the indicated times after saline or AAV8 ProMyo injection. E: Glucose uptake per unit muscle mass during an i/p glucose tolerance test (IPGTT) 2 weeks after saline or AAV8 ProMyo injection. Data are shown as mean + S.E.M. ** p<0.01 *vs*. Saline at the same time point. *** p<0.001 *vs*. Saline at the same time point. Two-way Repeated Measures ANOVA with Sidak-Holm posthoc test (A, C, D); Paired t-test (B, E).

Figure 2: Muscle insulin-stimulated glucose disposal is not affected by 2 weeks of myostatin inhibition in mice on a high fat diet

Body mass (A) and epididymal fat pad mass (B) of chow-fed and high fat diet (HFD)-fed mice after 2 weeks of intramuscular ProMyo overexpression (n=10 per group). C: Blood glucose concentration during IPITT. D: Normalized blood glucose concentration during IPITT. Data in A-D are shown as mean +/- S.E.M. E: Muscle mass in chow-fed and HFD-fed mice 2 weeks after saline or AAV8 ProMyo injection. F: Glucose uptake into TC muscle during the IPITT. Bars in E & F show mean values and data points connected by a line represent contralateral muscle pairs from the same animal. ** Indicates p<0.01 *vs*. control. *** Indicates p<0.001 *vs*. control. Unpaired t-test (A, B); Two-way Repeated Measures ANOVA with Sidak-Holm posthoc test (C, D, E, F)

Figure 3: Higher skeletal muscle insulin-stimulated glucose disposal after 10 weeks of myostatin inhibition in mice on a high fat diet

Body mass (A) and epididymal fat pad mass (B) of chow-fed and high fat diet (HFD)-fed mice after 10 weeks of intramuscular ProMyo overexpression (n=10 per group). C: Blood glucose concentration during IPITT. D: Normalized blood glucose concentration during IPITT. Data in A-D are shown as mean +/- S.E.M. E: Muscle mass in chow-fed and HFD-fed mice 10 weeks after saline or AAV8 ProMyo injection. F: Glucose uptake into TC muscle during the IPITT. Bars in E & F show mean values and data points connected by a line represent contralateral muscle pairs from the same animal. * Indicates $p<0.05$ *vs*. control. ** Indicates $p<0.01$ *vs*. control. *** Indicates $p<0.001$ *vs*. control. Unpaired t-test (A, B); Two-way Repeated Measures ANOVA with Sidak-Holm posthoc test (C, D, E, F).

Figure 4: Effect of 10 weeks of myostatin inhibition in HFD-fed mice on glucose transporter expression

A-C: Real-time PCR analysis of ProMyo (A), Slc2a1/GLUT1 (B) and Slc2a4/GLUT4 (C) transcript levels in chow- and HFD-fed mice (n=8 per group). A significant ANOVA main effect of ProMyo on GLUT1 transcript levels (B) is indicated. D & E: Western blot quantification of protein levels of GLUT1 (D, n=8 per group) and GLUT4 (E, n=7-8 per group). F: Example western blot images. Samples from intra-animal muscle pairs are indicated by lines underneath the blot images. ProMyo (+) or saline (-) treatment is indicated. Data are shown as mean + S.E.M. * $p<0.05$. ** $p<0.01$. *** $p<0.001$. Two-way Repeated Measures ANOVA with Sidak-Holm posthoc test (A-E).

Figure 5: Effect of 10 weeks of myostatin inhibition in HFD-fed mice on signalling pathways controlling glucose transporters

A-G: Western blot quantification of phospho- and total levels of Akt (A & B), AMPK (C & D), ACC (E & F), and PGC-1α protein (G) (n=6-8 per group). Significant ANOVA main effects of ProMyo on ACC levels (F) and of diet on PGC-1α levels (G) are indicated. H: Example western blot images. Samples from intra-animal muscle pairs are indicated by lines underneath the blot images. ProMyo (+) or saline (-) treatment is indicated. The vertical spaces between blot images indicate lanes that were on the same blot but from which other lanes have been cropped out. Data are shown as mean + S.E.M. * $p<0.05$. ** $p<0.01$. Two-way Repeated Measures ANOVA with Sidak-Holm posthoc test (A-G).

Figure 6: Effect of 10 weeks of myostatin inhibition in HFD-fed mice on insulin signalling-controlling E3 ligases

A-B: Real-time PCR analysis of MG53 (A) and Cblb (B) transcript levels in chow and HFD-fed mice (n=8 per group). C: Western blot quantification of Cbl-b protein levels (n=8 per group). Significant ANOVA main effects of ProMyo on MG53 transcript levels (A) and of diet on Cbl-b protein levels (C) are indicated. D: Example western blot images. Samples from intra-animal muscle pairs are indicated by lines underneath the blot images. ProMyo (+) or saline (-) treatment is indicated. Data are shown as mean + S.E.M. * $p<0.05$. Two-way Repeated Measures ANOVA with Sidak-Holm posthoc test (A, B, C).

Figure 7: Effect of 10 weeks of myostatin inhibition in HFD-fed mice on mitochondrial protein levels

A-C: Western blot quantification of nuclear-encoded complex III subunit UQCRC2 (A) and complex II subunit SDHB (B), and mitochondrially-encoded complex IV subunit MTCO1 (C) protein levels (n=8 per group). D: Example western blot images. Samples from intra-animal muscle pairs are indicated by lines underneath the blot images. ProMyo (+) or saline (-) treatment is indicated. Data are shown as mean + S.E.M. No significant differences were detected. Two-way Repeated Measures ANOVA with Sidak-Holm posthoc test (A, B, C).

Figure 1

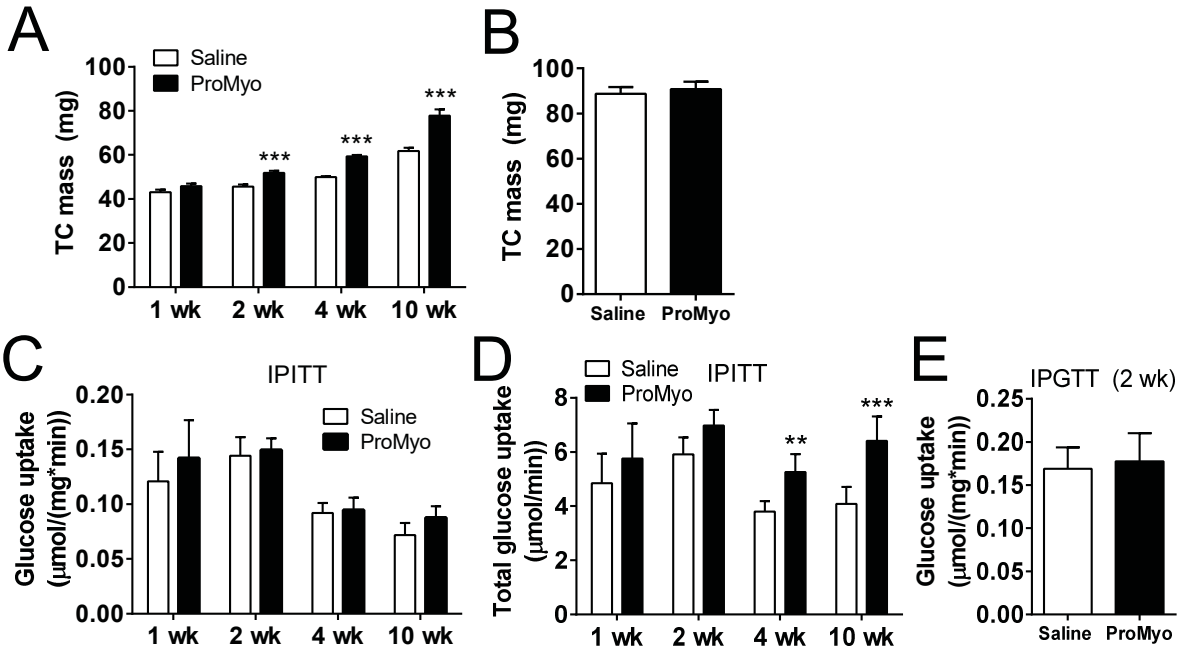
A
Saline
ProMyo
TC mass (mg)
100
80
60
40
20
0
***
***
***
1 wk
2 wk
4 wk
10 wk
B
TC mass (mg)
100
80
60
40
20
0
Saline
ProMyo
C
IPITT
Saline
ProMyo
Glucose uptake (µmol/(mg*min))
0.20
0.15
0.10
0.05
0.00
1 wk
2 wk
4 wk
10 wk
D
Saline
ProMyo
IPITT
Total glucose uptake (µmol/min))
8
6
4
2
0
**
***
1 wk
2 wk
4 wk
10 wk
E
IPGTT (2 wk)
Glucose uptake (µmol/(mg*min))
0.25
0.20
0.15
0.10
0.05
0.00
Saline
ProMyo

Figure 2

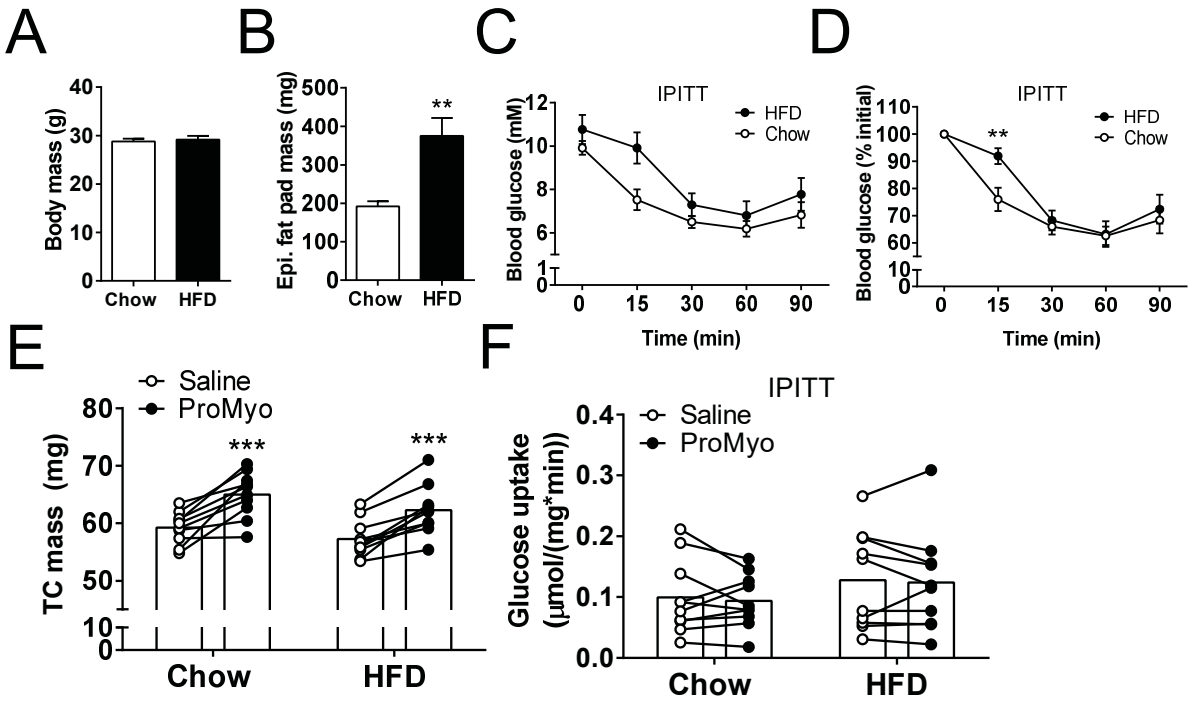
A
B
C
D
Body mass (g)
Chow
HFD
Epi. fat pad mass (mg)
**
IPITT
HFD
Chow
Blood glucose (mM)
Time (min)
Blood glucose (% initial)
E
F
Saline
ProMyo
TC mass (mg)
***
Glucose uptake (µmol/(mg*min))

Figure 3

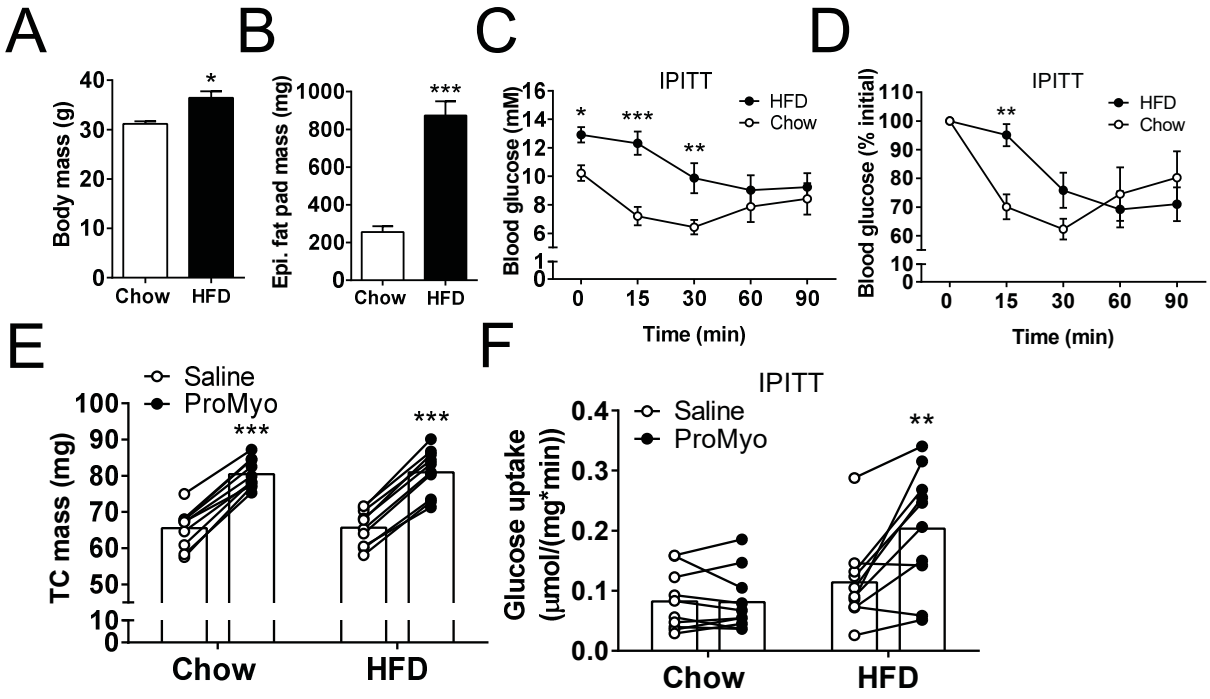
A
B
C
D
Body mass (g)
Chow
HFD
Epi. fat pad mass (mg)
IPITT
Blood glucose (mM)
Blood glucose (% initial)
Time (min)
HFD
Chow
E
F
Saline
ProMyo
TC mass (mg)
Glucose uptake (µmol/(mg*min))

Figure 4

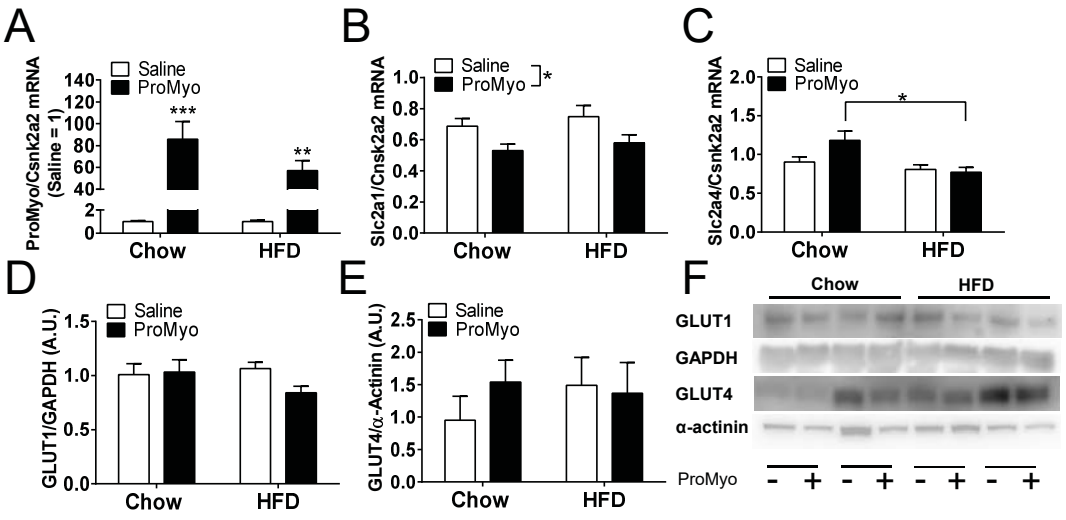
A
ProMyo/Csnk2a2 mRNA (Saline = 1)
Saline
ProMyo
***
**
Chow
HFD
B
Slc2a1/Cnsk2a2 mRNA
*
C
Slc2a4/Csnk2a2 mRNA
D
GLUT1/GAPDH (A.U.)
E
GLUT4/α-Actinin (A.U.)
F
GLUT1
GAPDH
GLUT4
α-actinin
ProMyo

Figure 5

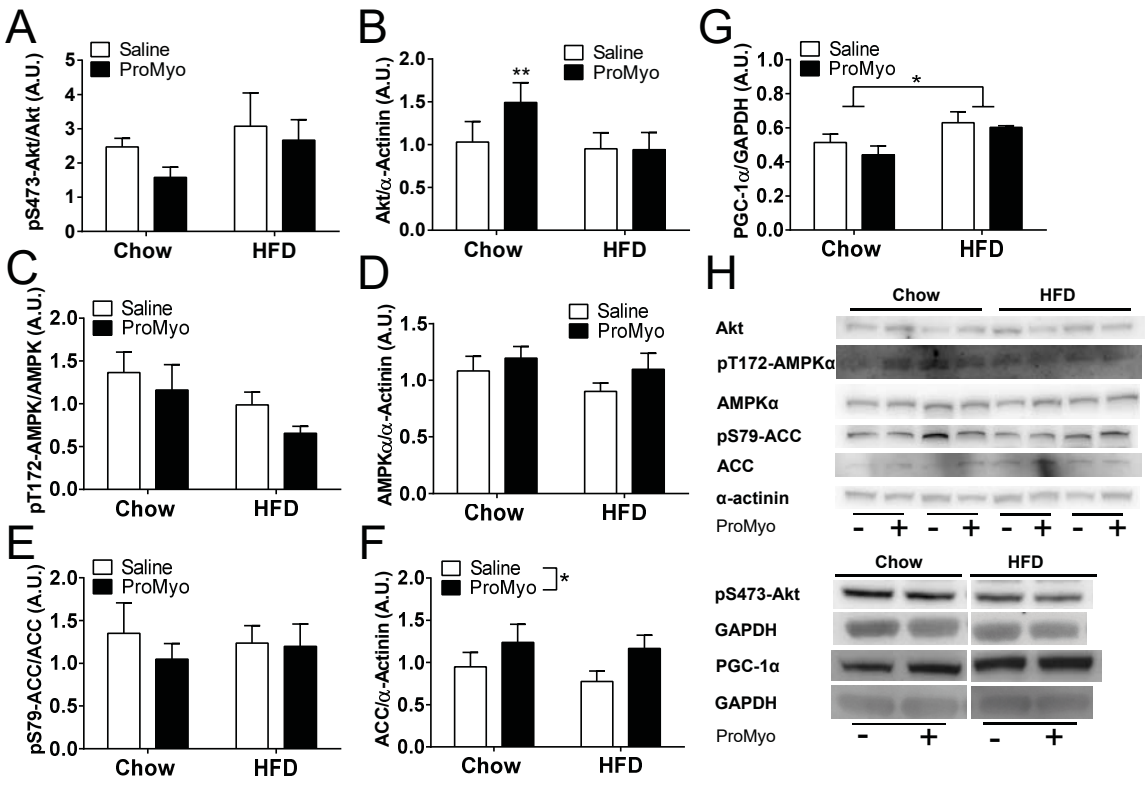
A
Saline
ProMyo
pS473-Akt/Akt (A.U.)
Chow
HFD
B
Saline
ProMyo
**
Akt/α-Actinin (A.U.)
Chow
HFD
G
Saline
ProMyo
*
PGC-1α/GAPDH (A.U.)
Chow
HFD
C
Saline
ProMyo
pT172-AMPK/AMPK (A.U.)
Chow
HFD
D
Saline
ProMyo
AMPKα/α-Actinin (A.U.)
Chow
HFD
H
Chow
HFD
Akt
pT172-AMPKα
AMPKα
pS79-ACC
ACC
α-actinin
ProMyo
- + - + - + - +
Chow
HFD
pS473-Akt
GAPDH
PGC-1α
GAPDH
ProMyo
- + - +
E
Saline
ProMyo
pS79-ACC/ACC (A.U.)
Chow
HFD
F
Saline
ProMyo
*
ACC/α-Actinin (A.U.)
Chow
HFD

Figure 6

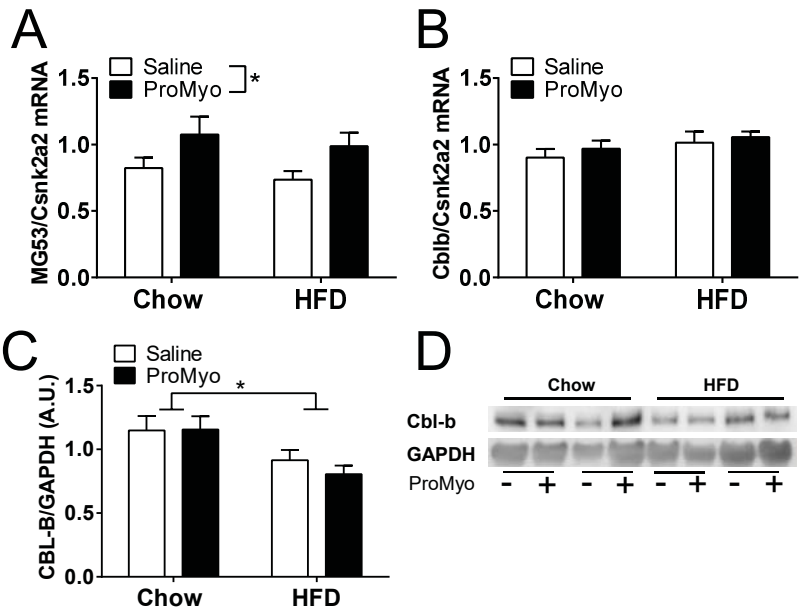
A
Saline
ProMyo
*
MG53/Csnk2a2 mRNA
1.5
1.0
0.5
0.0
Chow
HFD
B
Saline
ProMyo
Cblb/Csnk2a2 mRNA
1.5
1.0
0.5
0.0
Chow
HFD
C
Saline
ProMyo
*
CBL-B/GAPDH (A.U.)
1.5
1.0
0.5
0.0
Chow
HFD
D
Chow
HFD
Cbl-b
GAPDH
ProMyo
- + - + - + - +

Figure 7

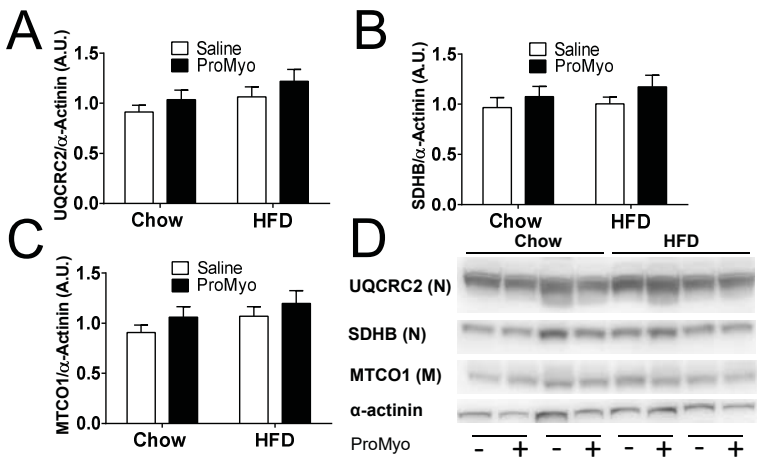
A
UQCRC2/α-Actinin (A.U.)
1.5
1.0
0.5
0.0
Saline
ProMyo
Chow
HFD
B
SDHB/α-Actinin (A.U.)
1.5
1.0
0.5
0.0
Saline
ProMyo
Chow
HFD
C
MTCO1/α-Actinin (A.U.)
1.5
1.0
0.5
0.0
Saline
ProMyo
Chow
HFD
D
Chow
HFD
UQCRC2 (N)
SDHB (N)
MTCO1 (M)
α-actinin
ProMyo
- + - + - + - +

Transcript	Primers	Reference
ProMyo	Fw: 5'-GGCACTGGTATTTGGCAGAG-3'	
	Rv: 5'-GTCCTGGGAAGGTTACAGCA-3'	
Mstn exon 1	Fw: 5'-TGTTTATATTTACCTGTTCATGCTGAT-3'	
	Rv: 5'-GCCCCTCTTTTTCCACATTTTC-3'	
Slc2a4/GLUT4	Fw: 5'-ACACTGGTCCTAGCTGTATTCT-3'	
	Rv: 5'-CCAGCCACGTTGCATTGTA-3'	
Slc2a1/GLUT1	Fw: 5'-CGGGGTCTTAAGTGCGTCAG-3'	
	Rv: 5'-CTCCCACAGCCAACATGAGG-3'	
MG53	Fw: 5'-TGTGTGCCTCGCTCGGTTC-3'	(31)
	Rv: 5'-TCTGCTTCACGGTCCAGAGAA-3'	
Cblb	Fw: 5'-GAGCCTCGCAGGACTATGAC-3'	(29)
	Rv: 5'-CTGGCCACTTCCACGTTATT-3'	

Table 1: Sequences of primers used for real-time RT-PCR analysis

Gene set	Size	ES	NES	FDR q value
KEGG_FATTY_ACID_METABOLISM	34	0.57	1.93	0.003
KEGG_OXIDATIVE_PHOSPHORYLATION	105	0.17	0.71	1.000
KEGG_INSULIN_SIGNALING_PATHWAY	123	0.16	0.68	0.970
GO_INFLAMMATORY_RESPONSE	454	-0.28	-1.39	0.145
GO_MACROPHAGE_ACTIVATION	31	-0.44	-1.43	0.172
GO_REGULATION_OF_MACROPHAGE_ACTIVATION	26	-0.35	-1.05	0.484
GO_MACROPHAGE_DIFFERENTIATION	19	-0.54	-1.56	0.128
GO_REGULATION_OF_MACROPHAGE_DIFFERENTIATION	20	-0.19	-0.57	0.986
GO_LEUKOCYTE_ACTIVATION	414	-0.22	-1.13	0.357
GO_T_CELL_MEDIATED_IMMUNITY	28	0.37	1.07	0.628
GO_REGULATION_OF_T_CELL_PROLIFERATION	147	0.23	0.98	0.504
GO_CYTOKINE_PRODUCTION	120	-0.22	-0.90	0.788
GO_CYTOKINE_MEDIATED_SIGNALING_PATHWAY	452	-0.24	-1.18	0.359
GO_TRANSLATIONAL_TERMINATION	86	0.53	2.14	0.024
GO_ORGANELLAR_RIBOSOME	68	0.55	2.12	0.020
GO_TRANSLATIONAL_ELONGATION	102	0.50	2.05	0.047
GO_MITOCHONDRIAL_TRANSLATION	95	0.50	2.05	0.036

Table 2: Gene set enrichment analysis of transcriptomics data from ProMyo overexpressing TA muscles of HFD-fed mice

Size: Number of genes in gene set; ES: Enrichment score; NES: Normalized enrichment score; FDR: False discovery rate (Significance threshold: $q<0.05$). Positive ES indicates enrichment of gene set in ProMyo-overexpressing muscles, negative ES indicates enrichment in saline-treated muscles.

Gene symbol	Gene title	Rank
ACSL3	acyl-CoA synthetase long-chain family member 3	7
ACSL4	acyl-CoA synthetase long-chain family member 4	251
ALDH9A1	aldehyde dehydrogenase 9 family, member A1	913
ECHS1	enoyl Coenzyme A hydratase, short chain, 1, mitochondrial	1,412
ACSL6	acyl-CoA synthetase long-chain family member 6	1,568
CPT1A	carnitine palmitoyltransferase 1A (liver)	1,781
ACADSB	acyl-Coenzyme A dehydrogenase, short/branched chain	1,973
ACADS	acyl-Coenzyme A dehydrogenase, C-2 to C-3 short chain	1,980
GCDH	glutaryl-Coenzyme A dehydrogenase	2,575
ACSL1	acyl-CoA synthetase long-chain family member 1	2,974
ACAA2	acetyl-Coenzyme A acyltransferase 2	3,095
HADHA	hydroxyacyl-Coenzyme A dehydrogenase, alpha subunit	3,181
ACADVL	acyl-Coenzyme A dehydrogenase, very long chain	3,187
HADH	hydroxyacyl-Coenzyme A dehydrogenase	3,398
ADH4	alcohol dehydrogenase 4 (class II), pi polypeptide	4,035
ACADL	acyl-Coenzyme A dehydrogenase, long chain	4,169

Table 3: Leading edge genes of KEGG_FATTY_ACID_METABOLISM gene set enriched in ProMyo-overexpressing vs. saline-treated muscles

Rank indicates the ranking of the gene in the list of all genes (total: 20,630) ranked on the basis of differential expression between ProMyo-overexpressing and saline-treated muscles.

Gene symbol	Gene title	Rank
MTG1	mitochondrial GTPase 1 homolog (S. cerevisiae)	202
GFM2	G elongation factor, mitochondrial 2	257
MRPS22	mitochondrial ribosomal protein S22	381
MRPS33	mitochondrial ribosomal protein S33	476
MRPL22	mitochondrial ribosomal protein L22	609
MTERFD2	MTERF domain containing 2	738
MRPS35	mitochondrial ribosomal protein S35	752
MRPS12	mitochondrial ribosomal protein S12	874
MRPL21	mitochondrial ribosomal protein L21	964
MRPS5	mitochondrial ribosomal protein S5	1,159
MRPL19	mitochondrial ribosomal protein L19	1,230
ABTB1	ankyrin repeat and BTB (POZ) domain containing 1	1,280
MRPS31	mitochondrial ribosomal protein S31	1,539
MRPL44	mitochondrial ribosomal protein L44	1,556
EIF5A2	eukaryotic translation initiation factor 5A2	1,745
MRPL3	mitochondrial ribosomal protein L3	1,759
TUFM	Tu translation elongation factor, mitochondrial	1,771
HARS	histidyl-tRNA synthetase	1,963
MRP63	mitochondrial ribosomal protein 63	2,008
MRPL18	mitochondrial ribosomal protein L18	2,017
MTRF1L	mitochondrial translational release factor 1-like	2,018
MRPS27	mitochondrial ribosomal protein S27	2,102
MRPL2	mitochondrial ribosomal protein L2	2,188
MRPL32	mitochondrial ribosomal protein L32	2,215
MRPL47	mitochondrial ribosomal protein L47	2,325
MRPS30	mitochondrial ribosomal protein S30	2,500
EEFSEC	eukaryotic elongation factor, selenocysteine-tRNA-specific	2,759
MRPL55	mitochondrial ribosomal protein L55	2,762
MRPL24	mitochondrial ribosomal protein L24	2,865
MRPS18A	mitochondrial ribosomal protein S18A	3,106
MRPL46	mitochondrial ribosomal protein L46	3,217

GFM1	G elongation factor, mitochondrial 1	3,349
MTIF2	mitochondrial translational initiation factor 2	3,428
EEF1D	eukaryotic translation elongation factor 1 delta	3,519
MRPL40	mitochondrial ribosomal protein L40	3,558
MRPS18C	mitochondrial ribosomal protein S18C	3,569
MRPS34	mitochondrial ribosomal protein S34	3,696
MRPS18B	mitochondrial ribosomal protein S18B	3,709
MRPS28	mitochondrial ribosomal protein S28	3,786
MRPS25	mitochondrial ribosomal protein S25	3,787
GSPT1	G1 to S phase transition 1	3,828
MRPS2	mitochondrial ribosomal protein S2	3,956
MRPL14	mitochondrial ribosomal protein L14	3,988
MRPS6	mitochondrial ribosomal protein S6	4,178
MRPL51	mitochondrial ribosomal protein L51	4,218
MRPS16	mitochondrial ribosomal protein S16	4,225
MRRF	mitochondrial ribosome recycling factor	4,419
MRPL54	mitochondrial ribosomal protein L54	4,603
EEF1A1	eukaryotic translation elongation factor 1 alpha 1	4,640
NSUN4	NOL1/NOP2/Sun domain family, member 4	4,659
MRPL20	mitochondrial ribosomal protein L20	4,671

Table 4: Leading edge genes of gene ontology-based gene sets enriched in ProMyo-overexpressing vs. saline-treated muscles

Rank indicates the ranking of the gene in the list of all genes (total: 20,630) ranked on the basis of differential expression between ProMyo-overexpressing and saline-treated muscles.